ACS OMEGA

Open Access

http://pubs.acs.org/journal/acsodf

Article

Direct Ink Writing of Strained Carbon Nanotube-Based Sensors: Toward 4D Printable Soft Robotics

Lana Joharji, Fahad Alam, and Nazek El-Atab*

Cite This: *ACS Omega* 2024, 9, 14638−14647

Read Online

ACCESS | Metrics & More | Article Recommendations | Supporting Information

ABSTRACT: Four-dimensional (4D) printing has attracted significant attention, because it enables structures to be reconfigured based on an external stimulus, realizing complex architectures that are useful for different applications. Nevertheless, most previously reported 4D-printed components have focused on actuators, which are just one part of a full soft robotic system. In this study, toward achieving fully 4D-printed systems, the design and direct ink writing of sensors with a straining mechanism that mimics the 4D effect are explored. Solution-processable carbon nanotubes (CNTs) were used as the sensing medium, and the effect of a heat-shrinkable shape-memory polymer-based substrate (i.e., potential 4D effect) on the electronic and structural properties of CNTs was assessed, followed by their application in various sensing devices. Herein, we reveal that substrate shrinking affords a more porous yet more conductive film owing to the compressive strain experienced by CNTs, leading to an increase in the carrier concentration. Furthermore, it improves the sensitivity of the devices without the need for chemical functionalization. Interestingly, the results show that, by engineering the potential 4D effect, the selectivity of the sensor can be tuned. Finally, the sensors were integrated into a fully 4D-printed flower structure, exhibiting their potential for different soft robotic applications.

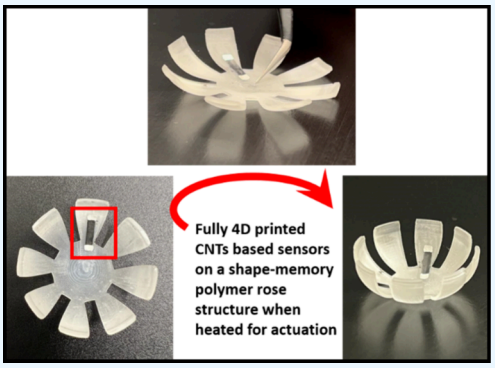

1. INTRODUCTION

In recent years, four-dimensional (4D) printing has attracted unprecedented attention owing to advances in additive manufacturing techniques, as well as responsive material design and development.[1] By combining active polymers with additive manufacturing, in addition to an appropriate mathematical model and sequential stimulations, 3D-printed structures can transition between various forms.[2] Hence, multifunctional materials and devices with complex designs can be printed with a wide range of applications from soft robotics to smart wearable devices, biomedical devices, and automobiles, to name a few. With this advancement, different active materials that can change in terms of shape, color, volume, features, or functionalities in response to extrinsic stimuli or environmental conditions have been explored for 4D printing.[3] These include shape-memory polymers (SMPs) in addition to their composites, dielectric elastomers, liquid crystal elastomers (LCEs), shape-memory alloys (SMAs), and hydrogels, all of which are currently available for 4D printing.[4] Such smart materials can respond to different stimuli, including heat,[1] electric[5] and magnetic fields,[6] light,[7] water,[8] and pH,[9] among others,[10] enabling the transformation of a 3D-printed structure into a 4D-printed one.

The majority of current 4D-printed structures focus on actuators with shape-changing abilities, such as stretching, flexing, corrugation, shrinking, and twisting, and their numerous applications in actuation. In fact, 4D printing combines the advantages of 3D printing (being rapid, cost-effective, and independent of advanced and complex fabrication processes) while offering flexibility in printing deformable structures with increased design complexity, cost reduction, and increased manufacturing efficiency.[11] Nevertheless, to achieve fully 4D-printed systems in the future, it is important to incorporate other functional devices such as sensors, memory, and logic devices.

Among smart materials, SMPs, LCEs, and hydrogels are very attractive owing to their ability to shrink with rapid response times, which enables their use in lifting objects,[12] folding,[13] and rolling functionalities.[14] The shrinking effect can be reversible or irreversible, depending on the application requirements. Several studies have reported inorganic sensors and electronic devices integrated on irreversibly shrinkable polymers. However, they are limited to using prestrained substrates to introduce the shrinking effect on the deposited active materials via various coating techniques. Moreover, they involve methods such as sputtering,[15] dip coating, and drop

Received: February 7, 2024
Revised: February 26, 2024
Accepted: February 29, 2024
Published: March 14, 2024

Table 1. Details of Previously Reported Strained Sensors

material	deposition technique	application	compatible with a fully 3D-/4D-printed system	reference
CNT/graphene oxide	vacuum filtration and transfer printing	strain sensor	no	Liu[36]
CNT	spray deposition	strain sensor	no	Park et al.[37]
CNT	transfer printing	strain sensor	no	Ma and Lu[38]
wrinkled chitosan/CNT	spray deposition	strain sensor	no	Zhang[39]
Ti/Au	physical vapor deposition	pressure sensor	no	Zeng[40]
CNT	direct Ink Writing	temperature, humidity, and pressure sensors	yes	this work

casting[16] and/or transferring of the prestrained substrate onto other permanent substrates, with no demonstrations so far of additively manufactured sensors that could be integrated into fully 4D-printed systems. Thus, the devices realized were mainly pressure and strain sensors in addition to electrochemical biosensors that require surface functionalization. For instance, Sando et al. fabricated graphene-based electrochemical sensors on a shrinkable polystyrene substrate using a dip coating technique followed by functionalization of the graphene layer.[17] Kim reported a gold-coated shrinkable polymer using the sputtering technique for blood pressure monitoring.[18] Woo et al. demonstrated a sputtered gold film on a shrinkable polymer with surface functionalization for DNA detection.[15] Wu et al. reported mercury sensors based on a shrinkable substrate with graphene mixed with gold nanoparticles with surface functionalization, which were coated using a combination of the sputtering and drop casting techniques.[16] Notably, the devices showed improved performance owing to either the increased surface area of the active materials or the generated cavities in the wrinkled continuous thin films.

Carbon nanotubes (CNTs) are exciting functional materials used for sensing because of their flexibility, stability, and outstanding physical and electronic properties. More specifically, CNTs can be solution processable. This enables their coating onto a wide range of substrates with a low thermal budget using a rapid and low-cost/low-waste technique, such as 3D printing via syringe dispensing, rendering them promising candidates for integration with fully 4D-printed structures. However, studies reporting on inorganic CNT-based electronic devices on shrinkable substrates are rare; furthermore, they are limited to strain sensors and are not compatible with 3D/4D printing. Park et al. reported a wrinkled CNT strain sensor fabricated via spray-gun deposition onto a shrinkable substrate, followed by transfer with an organic solvent onto an Ecoflex stretchable substrate, resulting in ultrastretchable strain sensors with excellent sensitivity.[19] The results were promising with extensive characterization of sensor performance; however, information about the structural and electronic properties of shrunk CNT films is limited. Thus, to date, no studies have reported 4D printable CNT-based sensors on smart, shrinkable substrates. Table 1 presents a comparison of the different reported strained sensors and their potential integration into fully 3D/4D printable systems. Notably, the different studies involve different units and techniques to calculate the sensitivity of the reported devices, rendering direct comparisons between the reported performances difficult.

In this study, temperature, humidity, and pressure sensors using solution-processable CNTs were fabricated on a shrinkable substrate. The active layers of the sensor were directly ink-written using a syringe dispensing to enable their integration into fully 4D-printed systems. 3D printing of shrinkable polymers such as LCEs has been previously demonstrated[4] and can result in a fully 3D-/4D-printed system if used as a substrate. The shrinking effect on the CNT film, including the charge-carrier density, mobility, resistivity, and porosity, was analyzed extensively. The performance of the resulting sensor is explained based on the new properties of the strained CNTs. More specifically, the results show that the shrinking effect can be engineered to improve the sensitivity of the devices owing to the more conductive yet more porous CNT film. In addition, the selectivity of the humidity sensor could be tuned using specific shrinking effects without the need for any surface functionalization or encapsulation. Finally, a fully 4D-printed flower with integrated CNT-based sensors is presented. This study represents a significant step toward the development of fully 4D-printed systems.

2. MATERIALS AND METHODS

2.1. CNT Channel Characterization. The channel dimensions were measured by using a Zeiss Axio Examiner Z1 microscope. The thickness of the CNT mesh was observed by using scanning electron microscopy (SEM) cross-sectional imaging. The compressive strain effect was observed using Raman spectroscopy, which was performed using an alpha300 apyron microscope with a 532 nm laser. The electronic properties of the CNTs, including carrier density, resistivity, and mobility, were measured using a Lake Shore Hall measurement system (Model 7704A). Porosimetry tests were conducted using a high-resolution 3Flex 3500 (Micromeritics) adsorption instrument with three 0.1 Torr pressure transducers and a high-vacuum system. The measurement was performed at −196 °C using a liquid N_2 bath, while sorption measurements were conducted using ultrahigh-purity nitrogen gas (99.999%). The samples, having a weight of ∼200 mg, were degassed for 12 h under a strong vacuum of 1 μ torr at room temperature before testing. Using the multipoint Brunauer−Emmett−Teller method, the specific surface area was extracted in the relative pressure range of $0.01 < P/Po < 0.1$. The porosity was measured before and after heating for 3 min at 110 °C via mercury intrusion porosimetry (MicroActive AutoPore V 9600 2.03.00, USA).

2.2. Sensor Fabrication and Characterization. The sensors were fabricated by using a fast-drying silver paint (Ted Pella) and P3-SWNT (Carbon Solutions). A Hydra 16A 3D printer was used to print the silver electrical contacts and CNT-based channels. A 3 mg amount of CNTs was mixed with 1 mL of isopropyl alcohol (IPA) to lower the concentration of the CNT solution, which was sonicated in

https://doi.org/10.1021/acsomega.4c01171
ACS Omega 2024, 9, 14638−14647

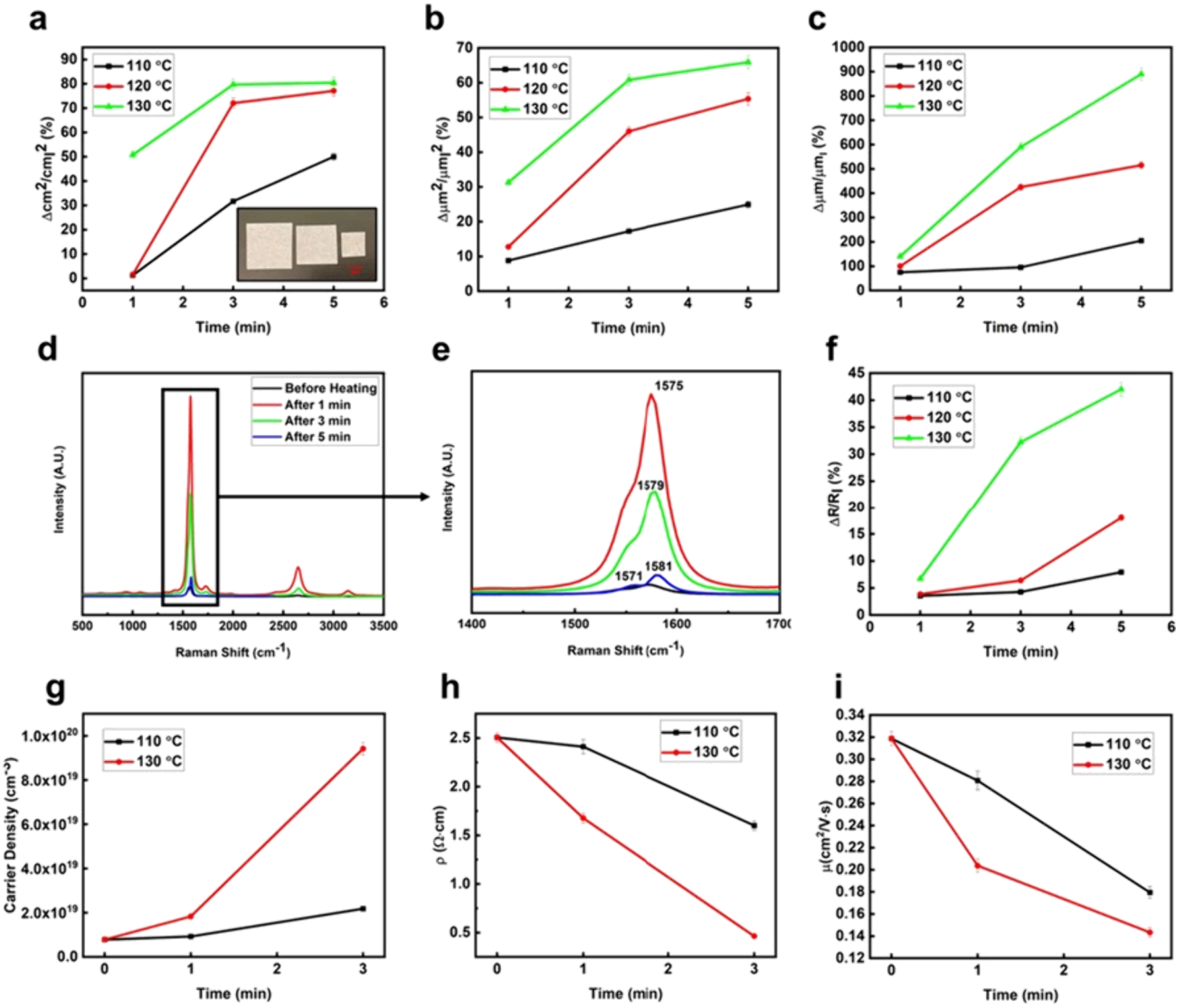

Figure 1. (a) Relative change in shrinkable substrate area for different samples at different temperatures and durations. Inset shows a photo of the shape-memory substrate after heating and shrinking (scale bar 1 cm). (b) Relative change of channel area due to shrinking upon heating at different temperatures and durations. (c) Relative change in CNT thickness after the shrinking effect. (d) Raman spectrum of CNTs at room temperature, after heating the shape-memory polymer substrate at 110 °C. (e) Magnification of Raman peaks at 1400−1700 cm^{-1} after heating at 110 °C. (f) Relative change in the resistance of the CNTs after the substrate shrinking effect; the resistance of the CNT channel decreases with the shrinking effect, whereas the relative change (plotted) increases. (g) Carrier density of CNTs before heating and after substrate shrinking. (h) Resistivity of CNTs and (i) mobility of CNTs after substrate shrinking at 110 and 130 °C for 1 and 3 min.

an ultrasonic bath (Branson) for approximately 2 h to disperse the CNTs. Using the direct-ink-writing approach in a 3D printer, a single layer of silver electrodes was dispensed first. Next, a single layer of CNTs was printed, which would be employed as the channel. The Hydra 16A printer uses a Repetrel software and requires G-codes to be developed using the PrusaSlicer software for the designs generated using the SolidWorks software. Moreover, a microprobe system (Nextron) was employed to examine the sensors at various temperatures, humidity, and pressure levels. The system was linked to a humidity control system, temperature controller, DI water, N_2 supply, pressure control system, vacuum pump, air supply, and a Keithley 4200A-SCS semiconductor device analyzer to read the DC resistance. The sensors were examined before and after the shrinking effect.

3. RESULTS

3.1. Fabrication and Characterization of CNT Channels on the Smart Substrate. The sensors were fabricated on heat-shrinkable shape-memory polymer-based substrates. The substrate consisted of thin, flexible sheets of polystyrene, which are typically used in do-it-yourself key chains. The sheets are sold prestretched by the manufacturer and shrink to their original size upon heating.[20] Initial tests were performed on a heat-shrinkable substrate to explore its behavior when exposed to various temperatures and for multiple durations before using it as a smart substrate in CNT-based resistive sensors. Figure 1a depicts the average relative change in area (i.e., $\frac{area_{before} - area_{after}}{area_{before}}$) of the smart substrate when the temperature is set to 110, 120, and 130 °C for 1, 3, and 5 min of heating. At a fixed temperature, the substrate area shrinks as the heating duration increases. For example, at 110 °C, the

https://doi.org/10.1021/acsomega.4c01171
ACS Omega 2024, 9, 14638−14647

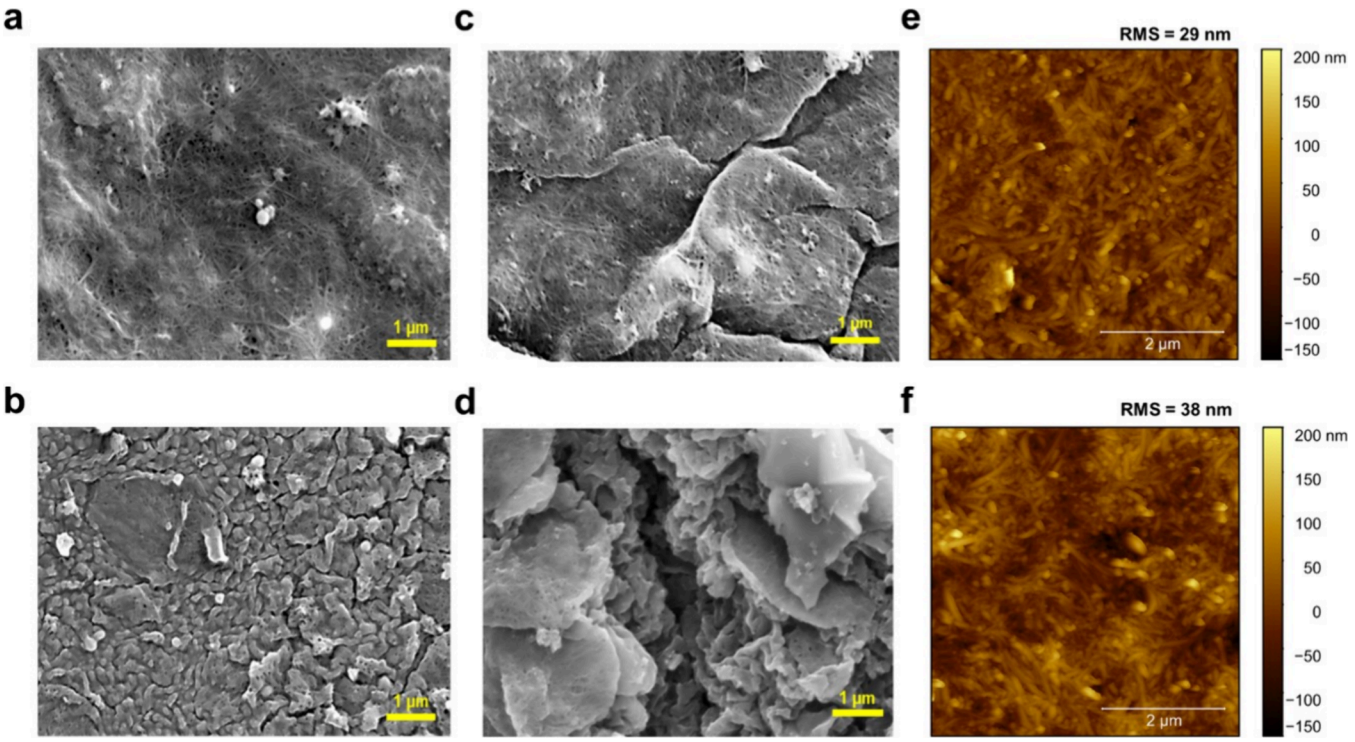

Figure 2. SEM images of the CNT film (a) before heating and (b) after the substrate shrinking effect at 110 °C for 3 min, (c) at 130 °C for 1 min, and (d) at 130 °C for 5 min. AFM images of the CNT mesh (e) before heating and (f) after the substrate shrinking effect at 110 °C for 3 min.

area decreased by 1.26 cm^2 as the heating duration increased to 3 min. In addition, for a fixed heating duration, the area of the substrate decreased as the heating temperature increased. For example, at 120 °C, the area decreased to 2.83 cm^2 after being heated for 3 min. In this study, the heat-shrinking effect was referred to as a 4D effect, as this would be the case if the smart substrate was printed.

Multiple characterization techniques were applied on CNTs to determine their different structural and electronic properties before and after the introduction of the shrinking effect. In this study, we used high-purity industrial-grade SWCNTs (Figure S1), which are 1/3 metallic and 2/3 semiconducting. The channel area of the CNTs was determined after applying the 4D effect; as with the substrate, the channel area was reduced either by raising the heating time for a fixed temperature or by raising the temperature for a fixed heating duration, owing to the substrate shrinking effect (Figure 1b and Figure S2). Heating at 120 °C for 1 min resulted in a decrease in channel area by ∼12.75%, whereas heating for 3 min reduced the channel area by ∼46.02% compared to the original value. In contrast, the thickness of the CNT mesh increased with substrate shrinkage (Figure 1c). The length and width of the channel were lowered after the shrinking effect; however, an increase in the thickness of the CNT mesh led to an overall rise in the volume of the channel, which can be attributed to the increase in its porosity and, thus, surface area. The relative change in thickness (i.e., $\frac{\text{thickness}_{\text{after}} - \text{thickness}_{\text{before}}}{\text{thickness}_{\text{before}}}$) was ∼75% when heating at 110 °C for 1 min, while heating at 130 °C for the same duration afforded a ∼140% change.

After the effect of the substrate on the dimensions and volume of the CNT mesh was measured, Raman spectroscopy was applied to determine whether the 4D effect caused strain within the mesh. The peaks of the CNTs after substrate shrinkage at different temperatures for different durations were identified, as shown in Figure 1d,e (Figure S3). Originally, the G peak of the CNT mesh was positioned at ∼1571 cm^{-1}.[21] After the 4D effect, the peak shifted to the right, suggesting that the CNTs experienced compressive stress. When the substrate was heated at 110 °C for 1 and 5 min, the peak shifted to ∼1575 and ∼1581 cm^{-1}, respectively. Notably, as the shrinking effect increased, the peak shifted further toward the right, confirming that a larger compressive strain developed within the mesh.

A compressive or tensile stress affects the electronic properties of the semiconductors. Thus, the electronic properties of the material were examined, including the resistance and resistivity as well as the carrier mobility and concentration, using the Hall effect measurement tool. The resistance measurements were first performed on the CNT-based channel, which was initially (i.e., before the 4D effect was applied) 7 mm wide and 2 mm long. To achieve electrical contact with the channel, silver ink was dispensed through a syringe dispenser by using a 3D printer. Figure 1f shows the relative change in electrical resistance (i.e., $\frac{R_{\text{before}} - R_{\text{after}}}{R_{\text{before}}}$) of the CNT channel when the substrate is heated for various durations and at multiple temperatures. As the shrinking effect increased (i.e., longer heating durations or temperatures), the resistance of the CNT channel decreased with an increase in the relative change. Additional characterization was performed using Hall measurements to analyze the strain effect on the material's conductivity.

As the shrinking effect, and therefore the compressive strain, increased, the CNT carrier density increased, while the mobility decreased. Moreover, under compressive strain, semiconducting CNTs transition from a semiconducting to a metallic state with a reduced bandgap.[22] Our findings can be

https://doi.org/10.1021/acsomega.4c01171
ACS Omega 2024, 9, 14638−14647

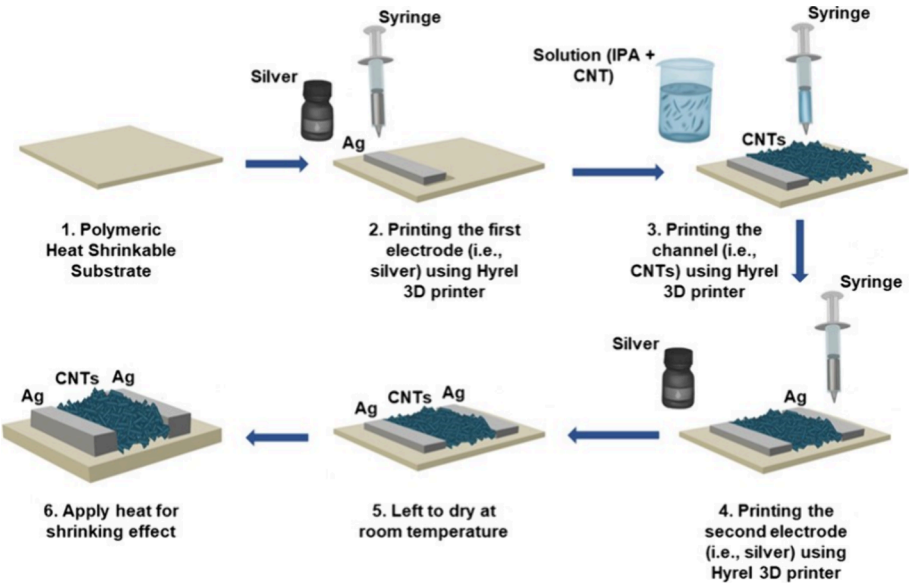

Figure 3. Detailed fabrication process of the 3D-printed CNT-based sensors using a syringe dispensing on a shape-memory polymer substrate.

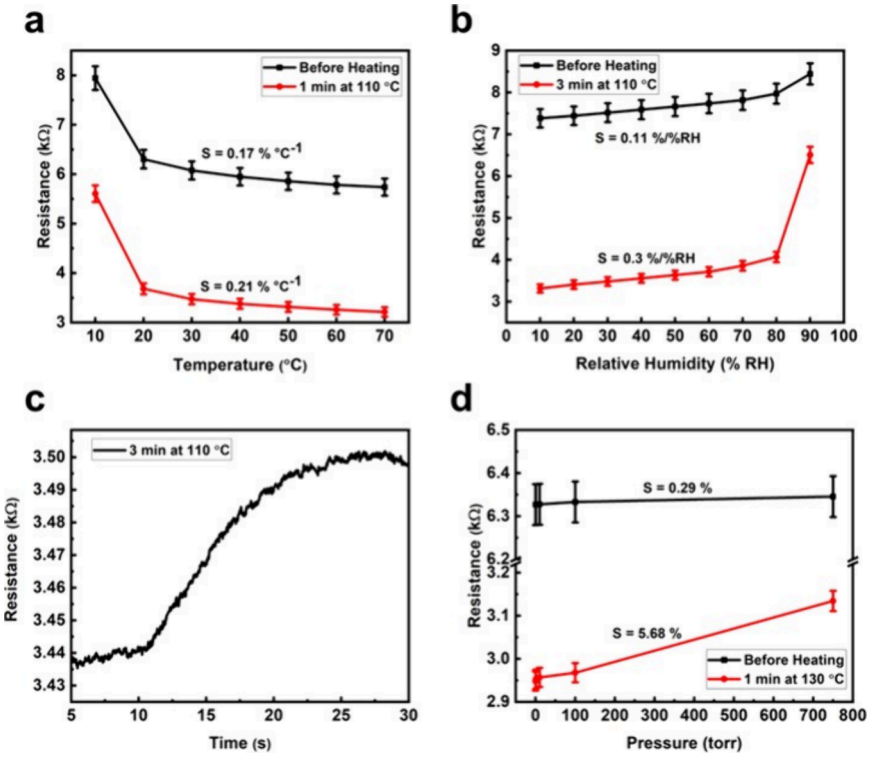

Figure 4. (a) Resistance−temperature relationship of the CNT sensors, using CNTs before heating vs after shrinking at 110 °C for 1 min. (b) Resistance−humidity relationship of the CNT sensors, using CNTs before heating vs after shrinking at 110 °C for 3 min. (c) Resistance−time relationship of the CNT humidity sensors at 110 °C for 3 min. (d) Resistance−pressure relationship of the CNT sensors, using CNTs before heating vs after shrinking at 130 °C for 1 min.

therefore attributed to the studied CNTs being 2/3 semiconducting. Moreover, owing to compressive strain, the percolation path in the CNTs network may vary, which can contribute to the observed results. Nevertheless, the overall resistivity of the material was reduced, suggesting that the influence of the carrier density is prevailing and overcompensates for the degradation of the mobility, resulting in an enhanced film conductivity. The carrier density increased from 7.83×10^{18} to 9.24×10^{18} and 1.83×10^{18} cm^{-3} upon shrinking the substrate via heating for 1 min at 110 and 130 °C, respectively (Figure 1g). All measurements were performed at room temperature after cooling the substrate. Although the resistivity and mobility decreased, the calculated relative change (i.e., $\frac{\rho_{before} - \rho_{after}}{\rho_{before}}$ or $\frac{\mu_{before} - \mu_{after}}{\mu_{before}}$) shows an incremental trend when the shrinking effect is aggravated, as depicted in Figure 1h,i. Moreover, the Hall effect measurements showed that the CNTs used were p-type, which is

https://doi.org/10.1021/acsomega.4c01171
ACS Omega 2024, 9, 14638−14647

expected as no treatment was applied, and thus, they were oxygen-doped in air.[23]

Scanning electron microscopy (SEM) and atomic force microscopy (AFM) images were obtained to study the surfaces of the CNT films at different temperatures and heating durations, as shown in Figure 2a−d. The SEM images depict that, as the shrinking effect is heightened (by raising the temperature or extending the heating duration), the porosity of the material increases. Cracks are observed at 110 and 120 °C beyond 3 min and at 130 °C for 1 min, as shown in Figure 2a−d. This further confirms that CNTs underwent compressive strain, owing to the shrinking effect. The AFM images of CNTs showed increased surface roughness with increased porosity (Figure 2e,f). This further supported the increase in volume upon shrinking. Finally, porosimetry tests were performed, revealing that the surface area of the CNT mesh was enhanced by ∼10 times when exposed to heat for 3 min at 130 °C, while the porosity increased from 14.53 to 20.53%. The increase in porosity was attributed to substrate shrinking due to an increase in volume, which further supports the finding of an increased CNT volume. Notably, the median volume pore diameter increased from 12.38 to 56.16 μm after shrinking, while the density $= \frac{\text{mass}}{\text{volume}}$ changed from 0.89 to 0.82 g/mL after heating at the same conditions. Subsequently, the sensing devices were 3D printed on a shape-memory polymeric substrate and extensively characterized.

3.2. Fabrication and Characterization of CNT Sensors.

After comprehensively examining the CNTs with the 4D effect (i.e., shrinking), the CNTs were utilized as a sensing medium for numerous stimuli, namely, temperature, humidity, and pressure. The sensitivity and selectivity of the sensors exposed to various 4D effects are assessed in the following sections.

The fabrication process flow and an optical image of the printed CNT-based sensor are presented in Figure 3 (Figure S4). More specifically, to develop the 3D-printed sensors, fast-drying silver paint and CNT solutions were used. The silver electrodes and CNT channel were 3D printed by using a Hyrel 3D system with syringe dispensing as previously explained.

The resulting sensor was tested as a temperature sensor. Figure 4a shows the resistance−temperature relationship for the device before and after heating for 1 min at 110 °C. The temperature was changed from 10 to 70 °C with a gradient of 10 °C for the original and shrunk sensors. The resistance of the CNTs decreased upon heating, which is expected for semiconducting materials. Although our CNTs were 1/3 metallic and 2/3 semiconducting, the results showed that the effect of the semiconducting CNTs was dominant. Furthermore, the smallest shrinking effect (i.e., heating at 110 °C for 1 min) resulted in a higher relative variation in resistance (i.e., $\frac{R_{\text{before}} - R_{\text{after}}}{R_{\text{before}}}$) and, thus, an enhanced sensitivity with respect to the original virgin sensor. Figure S5 shows the resistance−time relationship for the CNT-based resistive temperature sensors under the settings that resulted in the highest sensitivity (110 °C for 1 min). At 30 °C, the resistance of the shrunken device decreased by ∼5.73%, whereas the original sensor showed a decrease in resistance by ∼3.62%. Sensitivity was calculated based on $S = \frac{\Delta R}{R_0 \times (\Delta T)}$ where R_0, ΔR, and ΔT are the room temperature resistance of the sensor, and changes in the resistance and temperatures, respectively. The calculated sensitivity for the intact sensor was 0.17% °C^{-1}, while the shortened sensor with a minimal shrinking effect exhibited a sensitivity of 0.21% °C^{-1} (i.e., 1 min of heating at 110 °C). The shrunk sensors exhibited similar sensitivities with previously reported CNT-based temperature sensors, such as 0.24% °C^{-1} and 0.13% K^{-1},[24,25] without requiring large quantities of CNTs and any surface functionalization after being 3D printed. Nevertheless, when higher shrinking percentages were applied, the sensitivity significantly decreased compared to that of the initial intact sensor. In general, heating causes the charge-carrier concentration in semiconductors to increase, therefore decreasing the resistance. However, the application of compressive strain on the CNT mesh can also increase the charge-carrier concentration, as shown in this study. Notably, the effect of the strain on charge carriers has been previously studied, revealing that compressive strain lowers the band gap until a semiconducting-to-metallic transition can occur beyond a threshold strain value.[26] Thus, the enhanced performance witnessed for the temperature sensor upon shrinking at 110 °C for 1 min can be attributed to the bandgap reduction as a result of the compressive strain, further increasing charge carriers and thus increasing the variation in resistance with respect to the original virgin device. Nonetheless, the increased strain that the CNT mesh experiences at elevated shrinking percentages leads to an additional increase in the intrinsic charge-carrier concentration, as shown by the Hall effect measurements. This renders the increase in the carrier concentration due to heat as less impactful. Therefore, the degradation of the sensitivity of the sensor observed beyond 110 °C for 1 min can be explained by the rise in charge-carrier concentration due to strain being larger than the rise in charge carrier due to the heating effect, resulting in a reduced sensitivity.

Subsequently, the printed devices were tested as humidity sensors. Figure 4b depicts the resistance−humidity relationship for the humidity sensors before and after heating for 3 min at 110 °C. The humidity level was altered from 10 to 90% with a 10% step increment for the original and shrunk sensors; a constant chamber temperature of 20 °C was conserved. The resistance increased with an increasing humidification. In fact, owing to the porous mesh created by their hollow structure and entangled nanotubes, CNTs are admirable for adsorbing water vapor.[27] Moreover, it was witnessed that exposing the sensor to heat under different conditions, including: 1 min at 110, 120, and 130 °C and 3 min at 110 and 120 °C, leads to an increased relative variation in resistance (i.e., $\frac{R_{\text{after}} - R_{\text{before}}}{R_{\text{before}}}$) and, therefore, an enhanced sensitivity with respect to the original virgin sensor. At a relative humidity (RH) of 50%, the resistance of the shrunken device increased by ∼2.2% (after exposing the sensor to 110 °C for 3 min), whereas the original intact device showed an increase in resistance of only ∼0.97%. The measurements were performed at room temperature after the device was cooled. The sensitivity was calculated based on $S = \frac{\Delta R}{R_0 \times (\Delta\,\%\,\text{RH})}$ where R_0, ΔR, and Δ%RH are the room temperature resistance of the sensor, and variations in the resistance and relative humidity, respectively. The calculated sensitivities were 0.11%/%RH for the intact sensor and 0.3%/%RH for the shrunk sensor. The sensitivity of the shrunk sensors showed good results compared with previously reported CNT-based humidity sensors, such as 0.1%/%RH and 0.5%/%RH.[28,29] Therefore, the shrinking effect on the sensor results in an enhanced sensitivity without requiring a chemical treatment for the CNTs.[30] Because the shrinking

https://doi.org/10.1021/acsomega.4c01171
ACS Omega 2024, 9, 14638−14647

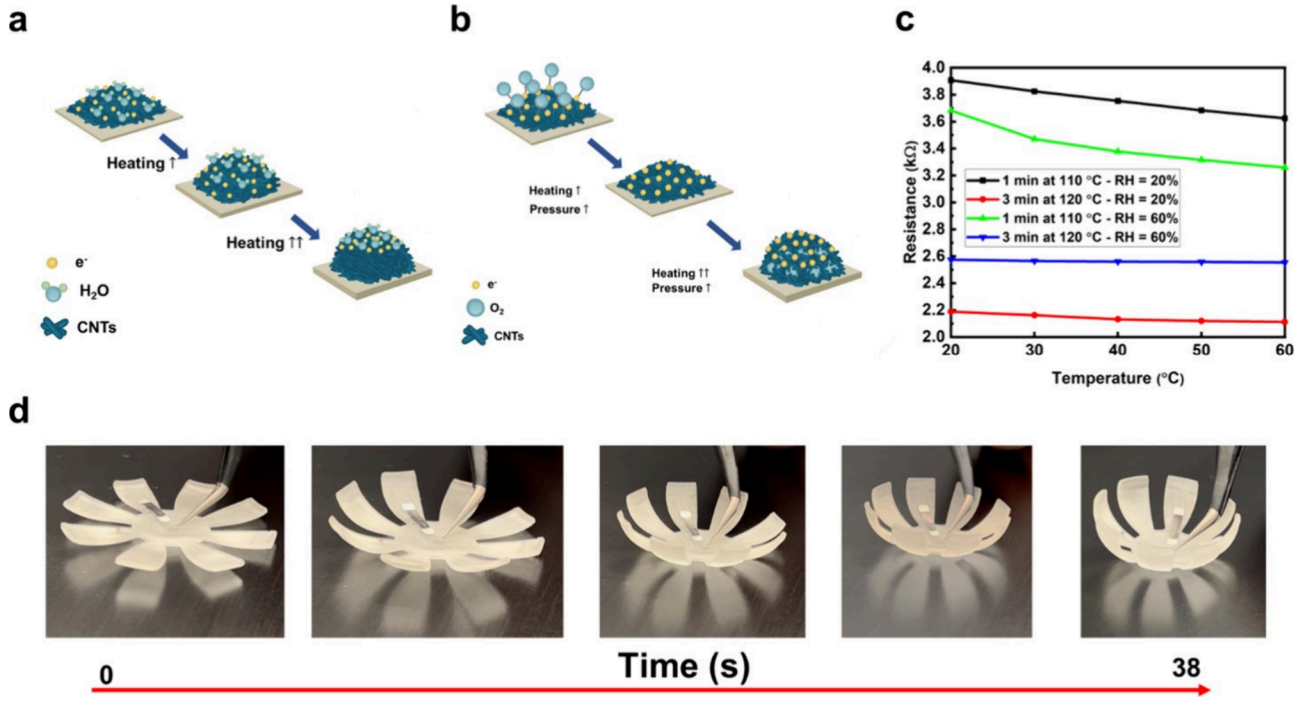

Figure 5. (a) Illustration of the humidity sensing mechanism: as the thickness of the CNT film increases due to larger shrinking effects, the sensitivity is reduced as it becomes more challenging for the H_2O molecules to reach the bottom area of the film. (b) Illustration of the pressure sensing mechanism: as the thickness of the CNT film increases due to larger shrinking effects, the sensitivity is reduced as it becomes more challenging for the trapped O_2 molecules in the bottom area of the CNT film to escape. (c) Resistance−temperature relationship of the humidity sensor for humidity-selective (1 min at 110 °C) and -nonselective (3 min at 120 °C) cases. (d) Fully 4D-printed CNTs on foldable petals.

effect improves the porosity of the CNT mesh (as earlier established by the porosity measurement and increased volume using SEM), the surface area of the CNT mesh increases, which enhances the sensitivity. Figure 4c depicts the resistance−time relationship for the humidity sensors that exhibited the highest sensitivity (110 °C for 3 min). The observed increase in resistance upon humidification can be explained by the following: when water molecules adhere to the CNTs, the carbon atoms on their surfaces donate electrons, which balance the hole carriers of the p-type CNTs, and therefore lead to a rise in their resistance. Additionally, adsorbed water molecules fill the spaces between the nanotubes and form nonconductive layers that obstruct the flow of electrons, eventually increasing the resistance. In other words, by increasing the humidity level, the adsorption of water molecules to the CNT surface increases, causing electron transfer and depleting the majority of charge carriers (holes) in the CNT network.[31]

Finally, the performance of the device as pressure sensors was explored. Figure 4d depicts the resistance−pressure relationship for the CNT-based pressure sensors before and after shrinking using 130 °C for 1 min. Pressure was set at 0.1, 1, 10, 100, and 750 Torr for the original and shrunk sensors at a constant temperature of 20 °C. The results showed that, when the pressure increased (toward atmospheric pressure), the resistance increased. Moreover, the several shrinking percentages (i.e., exposing the sensor to 110, 120, and 130 °C for 1 min and to 110 °C for 3 min) afforded increased relative changes in resistance (i.e., $\frac{R_{after} - R_{before}}{R_{before}}$) and, thus, higher sensitivities compared to the initial intact sensor. For example, a pressure of 100 Torr increased the resistance by ∼0.4% after exposing the sensor to 130 °C for 1 min, while the intact sensor showed an ∼0.08% resistance increase. The sensitivity was calculated based on $S = \frac{\Delta R}{R_0}$ where R_0 and ΔR are the room temperature resistance of the sensor and variations in the resistance, respectively. The calculated sensitivity was 0.29% for the original sensor and 5.68% for the shrunken sensor upon heating at 130 °C for 1 min. The sensitivity of the shrunk sensors was excellent compared to previously reported CNT-based pressure sensors, such as 11% and ∼0% at ∼30 °C.[32,33] Similarly, in the case of temperature and humidity sensors, the 4D effect led to a higher sensitivity without the need for predoping the CNTs to increase the defects that are already present, which would usually increase the sensitivity to changes in oxygen levels.[34] Moreover, the increase in CNT resistance at higher pressures can be attributed to the fact that O_2 holds some of the electrons at atmospheric pressure, giving the CNTs a specific resistance and making them p-type, with holes forming the majority of carriers. Therefore, upon a decrease in pressure, the material would become less p-type because the O_2 levels will decrease with the pressure, freeing up electrons.[35] However, this increase in electrons led to a reduction in the resistance, which could be due to the CNTs being 1/3 metallic.

Notably, beyond a specific shrinking percentage, the sensitivity of both the humidity and pressure sensors starts to decrease even though the porosity and volume continue to increase. In the case of the humidity sensor, this can be attributed to the greater thickness of the CNT mesh, which does not permit the water molecules to reach the bottom areas within the mesh; therefore, only the top part of the channel is impacted by the humidity, as shown in Figure 5a, resulting in an overall reduction in the sensitivity. In the case of the pressure sensor, the sensitivity drop can be attributed to the release of trapped and adsorbed O_2 from the bottom of the

https://doi.org/10.1021/acsomega.4c01171
ACS Omega 2024, 9, 14638−14647

thick CNT mesh by lowering the pressure (Figure 5b), thus causing smaller variations in resistance and therefore reduced sensitivity.

Based on the above results, the 3D-printed CNT sensor exhibits decent sensitivity to temperature for a given shrinking effect, whereas it becomes more sensitive to humidity and pressure for other shrinking percentages (Figure S6). This suggests that the selectivity of the sensor can be tuned based on the 4D shrinking effect. To confirm this, the optimized humidity sensor was tested at different temperatures (using the corresponding 4D shrinking effect) to demonstrate its humidity selectivity. As mentioned earlier, shrinking the sensor at 110 °C for 1 min resulted in the best temperature sensitivity (i.e., humidity-nonselective sensor), whereas shrinking the sensor at 120 °C for 3 min resulted in the highest humidity sensitivity (i.e., humidity-selective sensor). Figure 5c shows the resistance change of both humidity-selective and -nonselective sensors when the temperature was varied. Regarding the selective sensor, the change in its resistance is negligible regardless of the temperature variation, whereas the resistance difference becomes more apparent at different humidity levels. Thus, an optimized temperature sensor can be selective to temperature (over humidity) by encapsulating it, whereas an optimized humidity sensor would be readily selective to humidity (over temperature) due to the strain effect. This confirms that the shrinking effect not only improves the sensitivity of the device with respect to its original virgin state but also enables tuning of the selectivity of the sensor.

As a proof of concept, a fully 4D-printed CNT sensor was developed on a shape-memory polymeric substrate with a flower-like structure, as shown in Figure 5d. In this case, both the substrate and active layers of the sensor were 3D printed to realize a truly 4D-printed sensor. Upon heating, the petals fold; this feature can be used for various applications, such as gripping or packaging. Furthermore, folding induced strain within the CNT mesh, which could then be tuned (Figures S7−S9). This confirmed the potential of the developed 4D-printed sensing devices for various applications including robotic applications.

4. DISCUSSION

In this study, we demonstrate the significant impact of substrate shrinkage on the properties of CNTs. The observed decrease in the areas of the substrate and CNT channels, along with an increase in the thickness and volume of the CNT mesh, highlights the influence of the 4D effect induced by the heat-shrinkable substrate. The shift in the G peak of the CNT mesh in Raman spectroscopy suggests that CNTs experienced compressive stress owing to the shrinking effect, which is further evidenced by changes in electronic properties such as resistance, carrier density, and mobility. The transition of semiconducting CNTs to a more metallic state under compressive strain, as indicated by Hall effect measurements, explains the observed decrease in the resistance and the increase in the carrier density. The changes in the surface morphology of CNTs, as observed in the SEM and AFM images, along with the increase in the porosity and surface area support the findings of the increased volume of the CNT mesh. These results are significant because they provide insights into the behavior of CNTs under the influence of substrate-induced strain and stress, which has implications for the design and development of advanced sensing devices using shape-memory polymers and CNTs.

The temperature sensor exhibited a decreased resistance upon heating. This was attributed to the semiconducting nature of CNTs, with the improved sensitivity in the shrunken sensor explained by the bandgap reduction as a result of the compressive strain, which enhances the charge-carrier concentration. In the case of humidity sensing, the increase in resistance upon humidification is due to the adsorption of water molecules on CNTs, which affects electron transfer and charge-carrier depletion. The enhanced sensitivity of the shrinking sensor is linked to its increased porosity and surface area. For pressure sensing, the increase in resistance with pressure is explained by the interaction of O_2 with CNTs, which affects electron availability. The sensitivity variation in the shrunken sensors was attributed to the balance between the strain- and heating-induced charge-carrier concentration changes. This study also demonstrates the tunable selectivity of the sensor based on the shrinking effect; different shrinking conditions can optimize the sensitivity to temperature, humidity, or pressure. However, beyond certain shrinking percentages, a decrease in the sensitivity of humidity and pressure sensors was observed, possibly owing to the increased thickness of the CNT mesh, suggesting the need for future work to optimize the shrinking process to balance the sensitivity and structural changes.

5. CONCLUSIONS

In this study, the shrinking (4D) effect on printed sensors using direct-ink writing was examined in an attempt to contribute to fully 4D-printed systems. Carbon nanotubes were utilized as active materials in printed sensors owing to their favorable chemical, electronic, and mechanical characteristics. The 4D shrinking effect of the substrate increased the conductivity of the CNT mesh while enhancing its porosity. This was a result of the rise in charge-carrier density due to the strain experienced by CNTs, as observed by the Raman shifts. The printed temperature-, humidity-, and pressure-resistive CNT-based sensors exhibited improved performance, owing to the shrinking effect. Moreover, the 4D effect enabled tuning of the selectivity of the sensor, which is a key and desirable feature. Future studies will include the use of reversible smart substrates for a wider range of robotic soft robotic applications.

■ ASSOCIATED CONTENT

Data Availability Statement

Data supporting the findings of this study are available throughout the manuscript and supporting files.

Supporting Information

The Supporting Information is available free of charge at https://pubs.acs.org/doi/10.1021/acsomega.4c01171.

X-Ray photoelectron spectroscopy data of CNTs, Raman spectroscopy, images of the device showing dimensions of the channel, additional sensitivity tests of the sensors under different conditions, and pictures of the fully 4D-printed flower actuator with embedded CNT-based sensor (PDF)

■ AUTHOR INFORMATION

Corresponding Author

Nazek El-Atab − *SAMA Laboratories, Electrical and Computer Engineering, Computer Electrical Mathematical Science and Engineering Division, King Abdullah University of Science and Technology (KAUST), Thuwal 23955-6900,*

https://doi.org/10.1021/acsomega.4c01171
ACS Omega 2024, 9, 14638−14647

Saudi Arabia; orcid.org/0000-0002-2296-2003; Email: nazek.elatab@kaust.edu.sa

Authors

Lana Joharji − *SAMA Laboratories, Electrical and Computer Engineering, Computer Electrical Mathematical Science and Engineering Division, King Abdullah University of Science and Technology (KAUST), Thuwal 23955-6900, Saudi Arabia; Electrical Engineering, King Fahd University of Petroleum and Minerals (KFUPM), Dhahran 31261, Saudi Arabia*

Fahad Alam − *SAMA Laboratories, Electrical and Computer Engineering, Computer Electrical Mathematical Science and Engineering Division, King Abdullah University of Science and Technology (KAUST), Thuwal 23955-6900, Saudi Arabia*

Complete contact information is available at: https://pubs.acs.org/10.1021/acsomega.4c01171

Author Contributions

N.E. conceptualized the study. L.J. performed the experiments. N.E. and L.J. analyzed the data. L.J. and N.E. prepared the manuscript. F.A. assisted with the 4D printing of the flower. All authors have approved the written manuscript.

Notes

The authors declare no competing financial interest.

■ ACKNOWLEDGMENTS

The authors acknowledge the generous support of King Abdullah University of Science and Technology.

■ REFERENCES

(1) Ding, Z.; Yuan, C.; Peng, X.; Wang, T.; Qi, H. J.; Dunn, M. L.; et al. Direct 4D printing via active composite materials. *Sci. Adv.* **2017**, *3*, No. e1602890.

(2) Wu, J.-J.; Huang, L.-M.; Zhao, Q.; Xie, T. 4D Printing: History and Recent Progress. *Chin. J. Polym. Sci.* **2018**, *36*, 563−575.

(3) He, C.; Zhang, M.; Guo, C. 4D printing of mashed potato/purple sweet potato puree with spontaneous color change. *Innovative Food Science & Emerging Technologies* **2020**, *59*, No. 102250.

(4) Zhao, Q.; Zou, W.; Luo, Y.; Xie, T. Shape memory polymer network with thermally distinct elasticity and plasticity. *Sci. Adv.* **2016**, *2*, No. e1501297.

(5) Rodriguez, J. N.; Zhu, C.; Duoss, E. B.; Wilson, T. S.; Spadaccini, C. M.; Lewicki, J. P.; et al. Shape-morphing composites with designed micro-architectures. *Sci. Rep* **2016**, *6*, 27933.

(6) Kim, Y.; Yuk, H.; Zhao, R.; Chester, S. A.; Zhao, X. Printing ferromagnetic domains for untethered fast-transforming soft materials. *Nature* **2018**, *558*, 274−279.

(7) Yang, H.; Leow, W. R.; Wang, T.; Wang, J.; Yu, J.; He, K.; Qi, D.; Wan, C.; Chen, X.; et al. 3D Printed Photoresponsive Devices Based on Shape Memory Composites. *Adv. Mater.* **2017**, *29*, No. 1701627.

(8) Sydney Gladman, A.; Matsumoto, E. A.; Nuzzo, R. G.; Mahadevan, L.; Lewis, J. A. Biomimetic 4D printing. *Nat. Mater.* **2016**, *15*, 413−418.

(9) Nadgorny, M.; Xiao, Z.; Chen, C.; Connal, L. A. Three-Dimensional Printing of pH-Responsive and Functional Polymers on an Affordable Desktop Printer. *ACS Appl. Mater. Interfaces* **2016**, *8*, 28946−28954.

(10) Zolfagharian, A.; et al. Control-based 4D printing: Adaptive 4D-printed systems. *Appl. Sci.* **2020**, *10*, 3020.

(11) Moetazedian, A.; Allum, J.; Gleadall, A.; Mele, E.; Silberschmidt, V. V. A new hybrid additive manufacturing process to selectively control mechanical properties. *Addit Manuf* **2021**, *47*, No. 102337.

(12) Kotikian, A.; Truby, R. L.; Boley, J. W.; White, T. J.; Lewis, J. A. 3D Printing of Liquid Crystal Elastomeric Actuators with Spatially Programed Nematic Order. *Adv. Mater.* **2018**, *30*, No. 1706164.

(13) Yuan, C.; et al. 3D printed reversible shape changing soft actuators assisted by liquid crystal elastomers. *Soft Matter* **2017**, *13*, 5558−5568.

(14) Zhai, F.; et al. 4D-printed untethered self-propelling soft robot with tactile perception: Rolling, racing, and exploring. *Matter* **2021**, *4*, 3313−3326.

(15) Woo, S. M.; Gabardo, C. M.; Soleymani, L. Prototyping of wrinkled nano-/microstructured electrodes for electrochemical DNA detection. *Anal. Chem.* **2014**, *86*, 12341−12347.

(16) Wu, Z.; Jing, G.; Cui, T. Shrink-induced ultrasensitive mercury sensor with graphene and gold nanoparticles self-assembly. *Microsystem Technologies* **2019**, *25*, 11−17.

(17) Sando, S.; Zhang, B.; Cui, T. Shrink-induced graphene sensor for alpha-fetoprotein detection with low-cost self-assembly and label-free assay. *Frontiers of Mechanical Engineering* **2017**, *12*, 574−580.

(18) Kim, J.; et al. Soft Wearable Pressure Sensors for Beat-to-Beat Blood Pressure Monitoring. *Adv. Healthc Mater.* **2019**, *8*, No. 1900109.

(19) Park, S. J.; Kim, J.; Chu, M.; Khine, M. Flexible Piezoresistive Pressure Sensor Using Wrinkled Carbon Nanotube Thin Films for Human Physiological Signals. *Adv. Mater. Technol.* **2018**, *3*, No. 1700158.

(20) Hubbard, A. M.; et al. Shrink Films Get a Grip. *ACS Appl. Polym. Mater.* **2019**, *1*, 1088−1095.

(21) Androulidakis, Ch.; Koukaras, E. N.; Hadjinicolaou, M.; Galiotis, C. Non-Eulerian behavior of graphitic materials under compression. *Carbon N Y* **2018**, *138*, 227−233.

(22) Chu, Z.; Xu, B.; Liang, J. Direct Application of Carbon Nanotubes (CNTs) Grown by Chemical Vapor Deposition (CVD) for Integrated Circuits (ICs) Interconnection: Challenges and Developments. *Nanomaterials* **2023**, *13*, 2791.

(23) Yu, C.; Murali, A.; Choi, K.; Ryu, Y. Air-stable fabric thermoelectric modules made of N- and P-type carbon nanotubes. *Energy Environ. Sci.* **2012**, *5*, 9481−9486.

(24) Karimov, K. S.; Chani, M. T. S.; Khalid, F. A. Carbon nanotubes film based temperature sensors. *Physica E Low Dimens Syst. Nanostruct* **2011**, *43*, 1701−1703.

(25) Sibinski, M.; Jakubowska, M.; Sloma, M. Flexible temperature sensors on fibers. *Sensors* **2010**, *10*, 7934−7946.

(26) Sreekala, S.; Peng, X. H.; Ajayan, P. M.; Nayak, S. K. Effect of strain on the band gap and effective mass of zigzag single-wall carbon nanotubes: First-principles density-functional calculations. *Phys. Rev. B Condens Matter Mater. Phys.* **2008**, *77*, No. 155434.

(27) Zhu, P.; et al. Flexible and Highly Sensitive Humidity Sensor Based on Cellulose Nanofibers and Carbon Nanotube Composite Film. *Langmuir* **2019**, *35*, 4834−4842.

(28) Turkani, V. S.; Narakathu, B. B.; Maddipatla, D.; Bazuin, B. J.; Atashbar, M. Z. *P1FW.5 - A Fully Printed CNT Based Humidity Sensor on Flexible PET Substrate*. in 519−520 (AMA Service GmbH, 2020). DOI: 10.5162/imcs2018/p1fw.5.

(29) Liu, L.; et al. Humidity sensitivity of multi-walled carbon nanotube networks deposited by dielectrophoresis. *Sensors* **2009**, *9*, 1714−1721.

(30) Cao, C. L.; Hu, C. G.; Fang, L.; Wang, S. X.; Tian, Y. S.; Pan, C. Y.; et al. Humidity sensor based on multi-walled carbon nanotube thin films. *J. Nanomater* **2011**, *2011*, 1.

(31) Turkani, V. S.; Narakathu, B. B.; Maddipatla, D.; Bazuin, B. J.; Atashbar, M. Z. *P1FW.5 - A Fully Printed CNT Based Humidity Sensor on Flexible PET Substrate*. in 519−520 (AMA Service GmbH, 2020) DOI: 10.5162/imcs2018/p1fw.5.

(32) Rajavel, K.; Dinesh, M.; Saranya, R.; Kumar, R. T. R. Enhanced vacuum sensing performance of multiwalled carbon nanotubes: Role of defects and carboxyl functionalization. *RSC Adv.* **2015**, *5*, 20479−20485.

(33) Ahn, S. Il. High-temperature vacuum pressure sensor using carbon nanotubes. *Mater. Lett.* **2020**, *268*, No. 127643.
(34) Manohar, G. V. S.; Pandey, S.; Nanda, K. K. Low power consumption pressure sensor based on carbon nanotubes. in *AIP Conference Proceedings* vol. *2005* (American Institute of Physics Inc., 2018).
(35) Bridgman, P. W. *The Effect of Pressure on the Electrical Resistance of Certain Semi-Conductors*; Harvard University Press (1951) vol. *79*.
(36) Liu, D. et al. Wrinkled, cracked and bridged carbon networks for highly sensitive and stretchable strain sensors. *Compos Part A Appl. Sci. Manuf* (2022) *163*.
(37) Park, S.; Kim, J.; Chu, M.; Khine, M. Highly Flexible Wrinkled Carbon Nanotube Thin Film Strain Sensor to Monitor Human Movement. *Adv. Mater. Technol.* **2016**, *1*, No. 1600053.
(38) Ma, L.; Lu, W. Carbon nanotube film based flexible bi-directional strain sensor for large deformation. *Mater. Lett.* **2020**, *260*, No. 126959.
(39) Zhang, B.; et al. A highly sensitive and stretchable strain sensor based on a wrinkled chitosan-multiwall carbon nanotube nano-composite. *J. Mater. Chem. C Mater.* **2021**, *9*, 14848−14857.
(40) Zeng, X.; et al. Tunable, Ultrasensitive, and Flexible Pressure Sensors Based on Wrinkled Microstructures for Electronic Skins. *ACS Appl. Mater. Interfaces* **2019**, *11*, 21218−21226.

https://doi.org/10.1021/acsomega.4c01171
ACS Omega 2024, 9, 14638−14647